Harmonic distortion and unbalance analysis in multi-inverter photovoltaic systems

Harmonic distortion and unbalance analysis in multi-inverter photovoltaic systems

Filippo Spertino*, Gianfranco Chicco, Alessandro Ciocia, Gabriele Malgaroli, Andrea Mazza, Angela Russo
Politecnico di Torino, Energy Department "Galileo Ferraris", corso Duca Degli Abruzzi 24, 10129, Italy
* filippo.spertino@polito.it

***Abstract*—The growing penetration of distributed generation connected to the grid by power electronics converters can adversely affect the power quality. The capability of the system to host large harmonic distortions and unbalance in three-phase systems may be an issue. In case of Photovoltaic (PV) systems, the harmonic injection and unbalance are due to the transistors commutated by Pulse Width Modulation (PWM) inside the converters. Thus, power converters, to comply with the distortion limits, are equipped with filters, and control methodologies are even required for the compensation of power unbalance. In this paper, the main goal is the quantification of the impact of harmonic distortion on the unbalance. After the presentation of a theoretical approach to deal with harmonic distortion and unbalance by appropriate indicators, a PV system with multi-inverter configuration is tested. The measurements of power quality of the worst and the best converters are compared to the overall measurements of power quality for all the inverters.**

Keywords—photovoltaic systems; power quality; harmonic distortion; interharmonics; unbalance; symmetrical components

I. INTRODUCTION

In grid-connected or stand-alone Photovoltaic (PV) systems the power converters are key components. They permit to extract the maximum power from PV generators and to inject power into the grid. Their architecture differs as a function of the size and the number of the installed converters [1]. In the centralized configuration, inverters with high capacity, up to 500 kW, are connected to several (50–100) PV strings in parallel: each string is composed of 15–25 series-connected modules [2]. In this case, installation costs are reduced thanks to few converters. If each converter is equipped with a conventional Maximum Power Point Tracker (MPPT), it cannot properly work in case of partial shadings or module failures, because local MPPs arise besides the global MPP, and the PV system performance drops significantly [3]. An algorithm, able to trace the current-voltage (*I-V*) characteristic curves in a single sweep, can identify the global MPP [4]. The centralized configuration can be the best solution in case of multi-megawatt ground-mounted PV systems without shading problems. In other cases, it is diffuse the usage of centralized converters equipped with many MPPTs [5]. In [6] a 330 kVA inverter is equipped with six MPPTs, each of them connected with a portion of the PV field affected by shadows at different hours of the day. On the other hand, smaller converters have relatively lower efficiency and higher installation costs. In the micro-inverter configuration, each PV module is equipped with a single inverter installed on its rear side: an individual MPPT is present and shading losses are minimized [7]. Although the impact of the fault of a single module is minimum for the PV system performance, the higher number of converters leads to a higher installation cost. In addition, these converters may have a reduced life, because they are installed outdoor and are subject to a continuous thermal stress [8]. In small PV applications, such as residential plants, the impact of inverter price on the system cost is lower, and micro-inverters can be the optimal solution.

The multi-inverter layout can be the appropriate compromise between centralized and string inverters, because with 5 or 6 strings in parallel, the protections (blocking diodes and fuses) are avoided. This configuration requires multiple separate converters, each of them with one or two MPPTs for a rated power of few tens of kilowatt. With parallel connection of few PV strings, the consequent mismatch in the *I-V* curves is reduced and better performance in case of partial shadings. Moreover, this configuration permits to connect strings with different manufacturing process, orientation with respect to South, and number of modules per string: it may be the best solution in case of PV systems installed on buildings with no regular roofs [9]. Nevertheless, it is necessary to investigate if the high number of small PV converters strongly affects the power quality of the systems in terms of harmonics and unbalance.

In the present paper, the waveform quality is considered in the light of recent developments about the application of indicators in which the unbalance is taken into account in the definition of extended harmonic [10] or inter-harmonic [11] distortion indices. Then, an experimental analysis is performed by considering harmonics, inter-harmonics and unbalance issues in a building applied PV plant with rated power of about 600 kW and multi-inverter configuration. First, all the inverters are tested to identify the worst and the best one, in terms of harmonic current emissions. Then, the selected inverters are monitored to analyze harmonic distortion and unbalance at different operating conditions. The next sections of this paper are organized as follows. In the second section the theoretical aspects of harmonic distortion analysis are presented. The procedure and indicators to quantify unbalance are presented in the third section. The architecture of the PV system used as case study, the experimental setup and the results are discussed in the fourth section. The last section contains the conclusions.

II. HARMONIC DISTORTION ANALYSIS

The propagation of perturbations in AC grids is getting more and more important due to the connection of many power converters, as for DC loads (LED lamps and electronic equipment) or renewable generators (wind and PV systems).

Distortion of voltage and current waveforms is discussed in terms of harmonic and inter-harmonic components, calculated by a Fourier analysis on the measured signals. In particular, the Discrete Fourier Transform (DFT) method permits to elaborate voltage and current signals in the time domain calculating the corresponding harmonics and inter-harmonics contributions in the frequency domain.

In order to properly perform the DFT, following the prescription defined by the Standard IEC 61000-4-7 [12], it is recommended to analyze 10 periods for a fundamental frequency f_1=50 Hz and 12 periods for f_1=60 Hz. In both cases, the time window $T=1/\Delta f_z$=200 ms, where the variable z represents the frequency bands of width Δf_z = 5 Hz each.

Considering f_1=50 Hz, the amplitude and phase spectra are measured for each frequency band $z = 1, \dots, Z$. In [13] it has been shown the existence of a *consistency condition* under which the components at frequencies multiple of Δf_z are harmonics for the waveform at fundamental frequency $1/T$, and are inter-harmonics for the waveform to fundamental frequency f_1. Let us represent the harmonic orders referring to the fundamental frequency f_1 as $h = 1, \dots, H$, where H is the maximum harmonic order considered in the analysis, and $\Delta f_h = f_1$. For any integer $k \geq 0$, this consistency condition is:

$$Z = 10^k H \tag{1}$$

and the corresponding frequency relationship used with $k = 1$:

$$\Delta f_h = 10^k \Delta f_z \tag{2}$$

These formulae are valid in the Standard IEC 61000-4-7 for f_1=50 Hz, but they are not valid for f_1=60 Hz when the frequency bands are taken at 5 Hz.

In this paper, let us consider a system with fundamental frequency f_1=50 Hz, maximum harmonic order H = 40 [12], frequency band Δf_z =5 Hz, and Z = 400. Starting from a finite sequence of N samples $x_0, \dots, x_{N-1}$, with N > 800 (to guarantee the Nyquist sampling theorem), the DFT of this signal is a complex number defined, for any integer $z = 1, \dots, Z$ (i.e., considering only the entries of interest), as follows:

$$\bar{X}_z = \sum_{n=0}^{N-1} x_n e^{\left(-j\frac{2\pi zn}{N}\right)} \tag{3}$$

The aggregation of the spectral contributions calculated by the DFT into harmonic and interharmonic groups is recommended in [12]: the root mean square (r.m.s.) value of the harmonic group ($U_{h,g}$ for voltage and $I_{h,g}$ for current, respectively) is calculated as a function of the h-th spectral component by the DFT, but also of the previous and successive five adjacent components [14].

After the calculation of the harmonics, these data are used to calculate indicators to quantify distortion and compare the results. According to the prescription defined in Standards [12] and [15], the following indicators can be considered among the most important:

- The Total Harmonic Distortion (*THD*) is the ratio between the r.m.s. value of the sum of all the harmonic contributions (U_h for voltage signals and I_h for current signals, respectively) up to a specified maximum harmonic order H and the r.m.s. value of the fundamental component (U_1 for voltage and I_1 for current, respectively). The fundamental components U_1 and I_1 can be either the measured values or the rated values:

$$THD_U = \frac{\sqrt{\sum_{h=2}^{H} \left(U_h\right)^2}}{U_1}, \quad THD_I = \frac{\sqrt{\sum_{h=2}^{H} \left(I_h\right)^2}}{I_1} \tag{4}$$

- The Group Total Harmonic Distortion (*THDG*) is the ratio between the r.m.s. value of the harmonic groups up to a defined maximum harmonic order H and the r.m.s. value of the group associated with the fundamental component ($U_{1,g}$ for voltage and $I_{1,g}$ for current, respectively)

$$THDG_U = \frac{\sqrt{\sum_{h=2}^{H} \left(U_{h,g}\right)^2}}{U_{1,g}}, \quad THDG_I = \frac{\sqrt{\sum_{h=2}^{H} \left(I_{h,g}\right)^2}}{I_{1,g}} \tag{5}$$

- The Partial Weighted Harmonic Distortion (*PWHD*) is the ratio between the r.m.s. value of the harmonic contributions higher than the 14th order and lower than the maximum harmonic order H, multiplied by the harmonic order h, and the fundamental one:

$$PWHD_U = \frac{\sqrt{\sum_{h=14}^{H} h \cdot (U_h)^2}}{U_1}, \quad PWHD_I = \frac{\sqrt{\sum_{h=14}^{H} h \cdot (I_h)^2}}{I_1} \tag{6}$$

- The Quadratically Weighted Total Harmonic Distortion (*QWTHD*) parameter is defined in [16]. It is the average of the *THD* values, weighted by the square r.m.s. values of the phase quantities. With respect to the previous indicators, calculated separately for the single phases, this parameter permits to quantify the equivalent harmonic distortion of unbalanced three-phase (a, b, c) systems.

$$QWTHD_U = \frac{U_a^2 \cdot THD_{I_a} + U_b^2 \cdot THD_{I_b} + U_c^2 \cdot THD_{I_c}}{U_a^2 + U_b^2 + U_c^2 \cdot} \tag{7}$$

$$QWTHD_I = \frac{I_a^2 \cdot THD_{I_a} + I_b^2 \cdot THD_{I_b} + I_c^2 \cdot THD_{I_c}}{I_a^2 + I_b^2 + I_c^2 \cdot} \tag{8}$$

In low and medium voltage distribution systems, the Standard EN 50160 defines general limits for the supplier, in terms of quality of voltage under normal operating conditions [17]. Regarding the total harmonic distortion, the maximum value for THD_U is 8%. Furthermore, it provides maximum values of individual harmonic voltages (up to 25th); for example, the fifth and seventh harmonics cannot exceed 6% and 5% of the fundamental voltage, respectively.

III. Unbalance Analysis Including Harmonic Distortion

Unbalance conditions regarding current and voltage signals can produce several consequences to the grid. In particular, some of the most diffuse problems are an increase in losses in phase and neutral conductors, a reduced performance of induction and synchronous machines and malfunctioning of electronic components. In case of PV generators, they can be studied as ideal current sources and the unbalance regarding current signals is studied in depth.

According to [18], in order to calculate the unbalance indicators, two possible methods are considered. In the first method, used in the present paper, indicators are calculated starting from variables transformed into symmetrical components. The second method calculates unbalance indicators from variables not transformed into symmetrical components (Non-SCs). The Symmetrical Component-Based (SCB) method [19] permits to simplify the unbalance analysis by changing a three-phase unbalanced system into two sets of balanced phasors, called positive and negative sequences, and a set of single-phase phasors, called the zero-sequence components. The analysis of the unbalance system, in the symmetrical component domain, permits to convert the results back to the phase domain. In order to work with symmetrical components, it is used the operator $\alpha = e^{j2\pi/3}$ to define the SC transformation matrix **T** [20]. It converts the signals in the SCs values $\bar{I}_{T1}^{(h)}$, $\bar{I}_{T2}^{(h)}$ and $\bar{I}_{T3}^{(h)}$ defined, for the harmonic h = 1,…, H, as:

$$\left| \bar{I}_{T1}^{(h)} \bar{I}_{T2}^{(h)} \bar{I}_{T3}^{(h)} \right|^T = \mathbf{T} \cdot \left| \bar{I}_a^{(h)} \bar{I}_b^{(h)} \bar{I}_c^{(h)} \right|^T \tag{9}$$

In a balanced system the following conditions occur, for any integer $m > 0$:

- for harmonic orders h=3m-2 (h=1, 4, 7…), only positive-sequence contributions can be nonzero,
- for harmonic orders h=3m-1 (h=2, 5, 8…), only negative-sequence contributions can be nonzero,
- for harmonic orders h=3m-3 (h=3, 6, 9…), only zero-sequence contributions can be nonzero,

while in unbalanced systems these conditions are not satisfied.

From the transformed current contributions, the balance phase current component $I_p^{(b)}$, the unbalance component $I_p^{(u)}$ and the distortion component $I_p^{(d)}$ are calculated as [16]:

$$I_p^{(b)} = \sqrt{\sum_{m=1}^{M} \left[\left(I_{T1}^{(3m-2)} \right)^2 + \left(I_{T2}^{(3m-1)} \right)^2 + \left(I_{T3}^{(3m-3)} \right)^2 \right]} \tag{10}$$

$$I_p^{(u)} = \sqrt{\sum_{m=1}^{M} \left[\begin{array}{l} \left(I_{T2}^{(3m-2)} \right)^2 + \left(I_{T3}^{(3m-2)} \right)^2 + \left(I_{T1}^{(3m-1)} \right)^2 + \\ \left(I_{T3}^{(3m-1)} \right)^2 + \left(I_{T1}^{(3m-3)} \right)^2 + \left(I_{T2}^{(3m-3)} \right)^2 \end{array} \right]} \tag{11}$$

$$I_p^{(d)} = \sqrt{\sum_{h=2}^{M}\left[\left(I_{T1}^{(h)}\right)^2 + \left(I_{T2}^{(h)}\right)^2 + \left(I_{T3}^{(h)}\right)^2\right]} \qquad (12)$$

Here the following indicators are considered:

- The Current Unbalance Factor (*CUF*) and Voltage Unbalance Factor (*VUF*): they are the ratios between negative and positive sequence components (r.m.s. values) at the fundamental frequency;
- The Total Phase Unbalance (TPU_I) parameter: it is the ratio between the unbalance component $I_p^{(u)}$ and the balance phase current component $I_p^{(b)}$. With respect to the traditional unbalance indicators, such as the *CUF*, it is introduced in [16] to better quantify the unbalance in case of distorted waveforms.

Thanks to symmetrical current components, it is possible to calculate another parameter, able to estimate the harmonic distortion in unbalanced systems. It is the Total Phase current Distortion (*TPD*) parameter and corresponds to a generalization of *THD* [16]:

$$TPD = \frac{I_p^{(d)}}{\sqrt{\left(I_{T1}^{(1)}\right)^2 + \left(I_{T2}^{(1)}\right)^2 + \left(I_{T3}^{(1)}\right)^2}} \qquad (13)$$

The above formulation has been indicated with respect to the harmonics $h = 1,\ldots, H$. The extension to interharmonics is carried out according to the approach indicated in [13], that leads to the following $\hat{TPD}$ formulation:

$$\hat{TPD} = \frac{\hat{I}_p^{(d)}}{\sqrt{\left(I_{T1}^{(10)}\right)^2 + \left(I_{T2}^{(10)}\right)^2 + \left(I_{T3}^{(10)}\right)^2}} \qquad (14)$$

Furthermore, the *TPU* has been extended in [13] by considering the ratio between the versions of the unbalance component $\hat{I}_p^{(u)}$ and the balance phase current component $\hat{I}_p^{(b)}$ defined by taking into account the interharmonics as in (1):

$$\hat{TPU} = \frac{\hat{I}_p^{(u)}}{\hat{I}_p^{(b)}} \qquad (15)$$

IV. EXPERIMENTAL ANALYSIS

A. System Architecture

The PV plant under test, with 600-kW nominal power, is installed on the roof of classrooms and the students' canteen of Politecnico di Torino university. It is connected to the AC grid by twenty-five inverters with a rated power of 20 or 25 kW. All the converters are equipped with two MPPTs, each of them managing a maximum of three parallel strings composed of 13 series-connected modules. This "multi-inverters" configuration is selected in order to better work in case of shadings. Actually, the roof is partitioned into several sheds which generate some shadows for short time. Regarding the PV modules with 20% efficiency, they are equipped with all-back-contact cells.

Fig. 1 View of the PV system under test

B. Experimental setup

The system for real-time data acquisition is the Automatic Data Acquisition System (ADAS) described in [21], allowing adequate accuracy of the on-line data (Fig. 2). The typical uncertainties of measurements, according to the deterministic approach, are ±0.1 % of the readings for voltage samples and ±0.5—1 % for current samples. Thus, the samples of instantaneous power are affected by about the same uncertainty (±0.5—1 %) of the current samples. The measurement system is composed of a PC notebook, a

multifunction data acquisition device and signal conditioning. This latter includes 3 voltage differential probes (range ±1000 V_{pk}), 3 current probes (Hall-effect with range ±200-2000 A_{pk}).

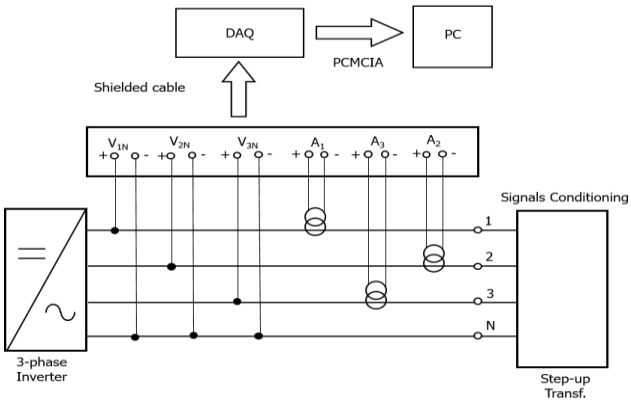

Fig. 2 Layout of the measurement system

C. Experimental results in terms of power quality

The procedure for data acquisition starts with the shut-down of the inverters: by opening the switches, it is possible to connect voltage probes and current clamps under safety conditions. They are connected to the signal conditioning of ADAS which is equipped with a software operating as digital oscilloscope/data logger. Before starting the measurements, the inverters are switched on and a few minutes are needed until their steady-state condition is reached. The acquisition of 10 waveforms is carried out for all the inverters in the PV system (a few devices were out of order), to identify the worst and the best converters, and the performance of the whole plant. Table I reports the distortion indicators calculated for current signals of all the tested inverters and of the entire plant. Then, only for the worst and best inverters (or units), the experimental signal analysis and processing lasted a complete day. In this way, the power quality parameters were calculated in various operating conditions from low power output up to a significant percentage of the rated power.

Fig. 3 shows the voltage and current waveforms of the worst converter (#7B) with the highest harmonic emissions at half output power. The distortion is mainly due to the fifth and the seventh order components and the $THD_I \approx 9\%$. As a comparison, Fig. 4 shows the voltage and current waveforms of the best converter (#9A) with the lowest harmonic emissions ($THD_I = 4\%$). Similarly to the #7B, the measured distortion on the #9A is due to the fifth and the seventh order components. In particular, the single harmonic contributions are reported in Fig. 5 and in Fig. 6. The two graphs refer to the r.m.s. values of ≈15 A and ≈18 A for the fundamental harmonic, respectively. They are truncated in the graphs to better show the higher order components. Of note is that the worst inverter presents a 250 Hz component twice the best one.

Considering the definition of *THD* in which the denominator is the fundamental harmonic of the current/voltage waveforms, the profiles of THD_I (#7B and #9A) are almost hyperbolic, while the profiles of THD_V are relatively constant [22]. In particular, the hyperbolic evolution of THD_I (with peaks higher than 30% at low load) derives from an almost constant numerator and a denominator quite proportional to the power output. The best inverter shows $THD_I \approx 4\%$, while the worst inverter exhibits $THD_I \approx 9\%$ at half power output.

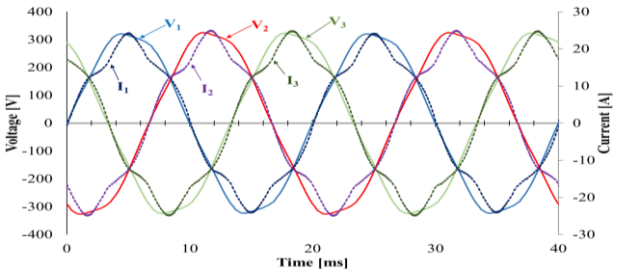

Fig. 3: Current and voltage waveforms of converter #7B

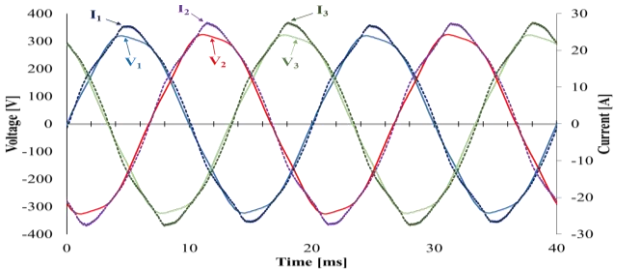

Fig. 4: Current and voltage waveforms of converter #9A

Fig. 5: Spectral analysis of current of converter #7B. The 50 Hz component (truncated in the graph) is 15.4 A

Fig. 6: Spectral analysis of current of converter #9A. The 50 Hz component (truncated in the graph) is 18.1 A

On the other hand, if the THD_I is normalized with respect to the rated value of the current (and thus the denominator is constant), it can be observed that the harmonic emission is quite constant for a well working device (#9A), while, for the worst converter, harmonics slightly increase with the power output (Fig. 8). The $QWTHD_I$ values are similar to single-phase *THD* values, therefore it is reasonable to expect low unbalance. Regarding the entire plant, the *THD* values for the individual phases are not identical to $QWTHD_I$, demonstrating the presence of a higher overall unbalance. This result is confirmed by the *TPD* indicators, whose values are similar to $QWTHD_I$ for each inverter and the entire plant.

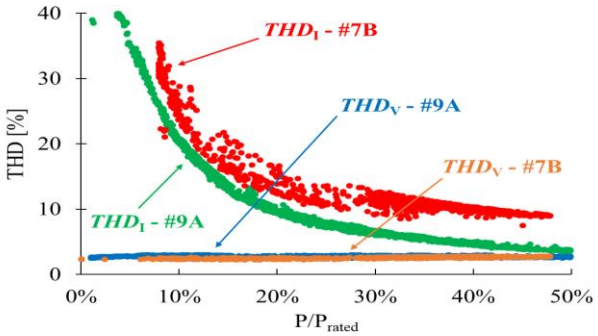

Fig. 7 THD values normalized with respect to the measured value of the fundamental harmonic for the two analyzed inverters.

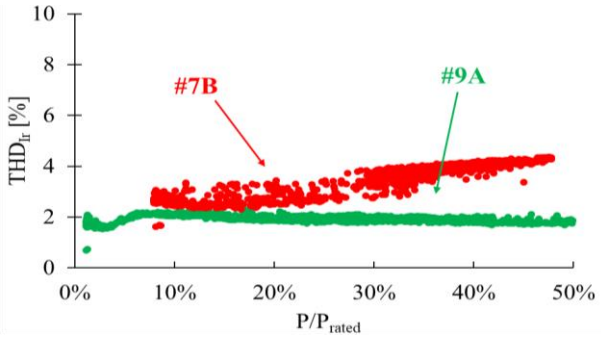

Fig. 8 THD_I values normalized with respect to the rated value of the fundamental harmonic for the two analyzed inverters.

TABLE I
SUMMARY OF DISTORTION INDICATORS

Unit	***TPD*** **[%]**	***TPD*** **[%]**	***QW-THD$_I$*** **[%]**	***PWHD*** **[%]**			***THD*** **[%]**		
				R	***S***	***T***	***R***	***S***	***T***
1A	7.4	4.7	4.7	0.9	1.0	0.8	4.6	4.7	4.7
2A	7.2	5.3	5.3	1.1	0.8	0.9	5.2	5.3	5.4
2B	6.1	4.4	4.4	1.3	1.3	1.6	4.4	4.3	4.5
3A	7.1	5.2	5.2	1.3	1.0	1.1	5.1	5.3	5.3
3B	7.9	5.7	5.7	1.1	1.0	1.0	5.6	5.7	5.8
4A	7.2	5.0	5.0	1.3	1.4	1.2	5.0	5.1	5.1
4B	6.5	4.3	4.3	1.2	1.1	1.3	4.2	4.3	4.4
5A	6.4	5.0	5.0	1.3	1.3	1.2	4.9	4.9	5.1
5B	6.1	4.4	4.3	1.3	1.2	1.2	4.3	4.2	4.5
6A	7.5	5.9	5.9	1.2	1.4	1.3	5.9	5.8	6.1
6B	8.2	6.1	6.1	1.3	1.2	1.1	6.1	6.1	6.1
7A	7.9	5.9	5.9	1.2	1.0	1.1	5.9	5.9	6.1
7B	**10.5**	**9.3**	**9.3**	**1.4**	**1.4**	**1.1**	**9.3**	**9.1**	**9.6**
8A	7.9	6.1	6.1	1.4	1.3	1.1	6.1	6.1	6.2
8B	7.1	5.2	5.2	1.4	1.1	1.1	5.2	5.1	5.5
9A	**6.6**	**3.9**	**3.9**	**1.0**	**0.7**	**0.9**	**3.9**	**3.9**	**4.0**
9B	8.1	6.2	6.2	1.1	1.1	1.0	6.2	6.1	6.3
10A	8.9	6.9	6.9	1.4	1.1	1.2	6.9	6.8	6.9
11A	8.0	5.6	5.6	1.1	0.8	0.9	5.5	5.5	5.7
12A	7.5	5.4	5.4	1.3	1.3	1.2	5.3	5.5	5.5
12B	6.4	5.0	5.0	1.0	0.8	0.9	4.9	5.0	5.0
12C	6.8	5.3	5.3	1.4	1.3	1.3	5.2	5.3	5.3
13A	6.4	5.1	5.1	5.2	7.6	5.4	5.0	5.2	5.2
Plant	11.9	7.1	7.0	0.9	1.0	0.8	7.8	6.9	6.4

TABLE II
SUMMARY OF THE UNBALANCE INDICATORS

Unit	*VUF [%]*	*CUF [%]*	*TPU$_I$ [%]*	*$\hat{TPU}_I$ [%]*
1A	0.21	0.74	1.08	5.4
2A	0.17	0.74	1.11	4.7
2B	0.16	0.62	1.22	4.1
3A	0.18	0.89	1.37	4.7
3B	0.22	0.75	1.13	5.3
4A	0.20	0.81	1.14	4.9
4B	0.17	0.66	1.23	4.7
5A	0.16	0.96	1.28	4.1
5B	0.14	0.88	1.34	4.2
6A	0.25	1.95	2.25	4.9
6B	0.22	3.13	3.72	6.2
7A	0.26	0.77	1.22	5.0
7B	**0.25**	**1.06**	**1.47**	**4.8**
8A	0.27	0.65	1.14	4.9
8B	0.26	0.61	1.13	4.7
9A	**0.25**	**0.68**	**1.23**	**5.2**
9B	0.25	0.91	1.49	5.0
10A	0.26	1.04	1.50	5.5
11A	0.25	1.02	1.58	5.5
12A	0.17	0.68	1.37	5.0
12B	0.15	0.62	0.95	4.0
12C	0.14	0.67	1.06	4.2
13A	0.13	0.48	1.03	3.8
Plant	0.27	3.25	5.75	9.71

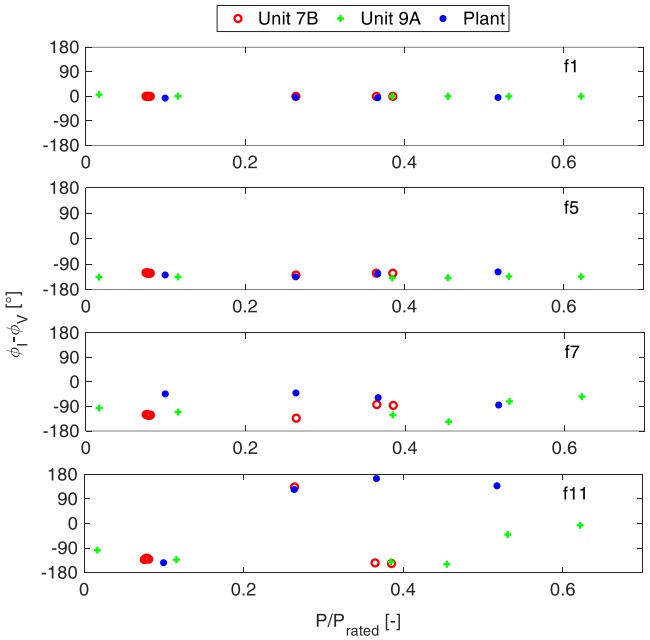

Fig. 9 Phase shift values for 1st, 5th, 7th and 11th harmonic orders as a function of the power output

Regarding the unbalance indicators, *VUF*, *CUF*, TPU_I and $\hat{TPU}_I$ values are shown in Table II. Voltage unbalance is very low (*VUF* ≈0.2%) and thus it respects EN 50160 limit (*VUF*≤2%). Regarding the currents, the unbalance effect on the entire plant is

higher than the effect on the individual converters: *CUF*≈3.3% for the plant and *CUF*≈0.5–3.1% for the single converters. It is argued that compensation is not present. This result is confirmed by the *TPU* values, which better quantify the unbalance in case of distorted waveforms: they are lower for the individual converters (*TPU*≈1.1–3.7%) with respect to the whole plant (*TPU*≈5.8%), even if the measurements are not simultaneous.

Analyzing in detail the results for the converter with the highest harmonic emission (#7B), the comparison between the traditional unbalance indicator *CUF* and the *TPU* parameter is highlighted. Its *CUF* value is not the highest in the whole plant (#6A and #6B are greater). The *TPU* ≈1.5 % of #7B is similar to the majority of those calculated for the other converters in the plant, while the worst TPU parameters are those of the abovementioned #6A and #6B converters *TPU*≈2↔4 %. Finally, Fig. 9 shows the phase shifts between current and voltage signals for units #7B and #9A and for the entire plants. Regarding the fundamental, the converters work at cos(φ) ≈1 and the variations are not significant. The higher harmonic orders exhibit phase shifts mainly within ±90°↔±180°; however, their contributions in terms of active power are negligible, due to low r.m.s. values.

V. CONCLUSIONS

In this paper, an analysis of the power quality in a PV system with multi-inverter configuration has been performed. Harmonic distortion indicators are calculated for each individual converter: the $QWTHD_I$ are almost identical to single-phase THD_I values, confirming low unbalance of currents. Regarding the entire plant, the single-phase THD_I values are not identical to $QWTHD_I$ (≈7 %), showing a not negligible overall unbalance. In addition, *TPD* provides similar values to QWTHD, confirming that the *TPD* well quantifies harmonic distortion in unbalanced systems. Concerning the unbalance, *CUF* is low (0.5%↔3.3%), but it is used to quantify the unbalance in a sinusoidal system. On the contrary, the *TPU* and $\hat{TPU}$ values, considering the harmonic distortion, are higher than *CUF* (*TPU* ≈ 1%↔6%; $\hat{TPU}$ ≈ 4%↔10 %). Finally, the unbalance in the whole plant tends to be higher than those of the individual converters. Therefore, the unbalance contribution of multiple inverters does not produce a self-compensation. In future works, the converters showing the highest unbalance will be studied in depth, to identify the causes and quantify the effects at different operating conditions.

REFERENCES

[1] S.B. Kjaer, J.K. Pedersen, and F. Blaabjerg, "A review of single-phase grid-connected inverters for photovoltaic modules," *IEEE Trans. on Industry Applications*, vol. 41, pp. 1292–1306, 2005.

[2] C. Meza, J.J. Negroni, D. Biel and F. Guinjoan, "Energy-Balance Modeling and Discrete Control for Single-Phase Grid-Connected PV Central Inverters," *IEEE Trans. on Industrial Electronics*, vol.55, no.7, pp. 2734–2743, 2008.

[3] F.Spertino, J. Ahmad, P. Di Leo, A. Ciocia, "A method for obtaining the I-V curve of photovoltaic arrays from module voltages and its applications for MPP tracking," *Solar Energy*, vol.139, pp. 489–505, 2016.

[4] F. Spertino, J. Ahmad, A. Ciocia and P. Di Leo, "A technique for tracking the global maximum power point of photovoltaic arrays under partial shading conditions," IEEE 6th International Symposium on Power Electronics for Distributed Generation Systems (PEDG), Aachen, 2015.

[5] H. Patel and V. Agarwal, "Maximum power point tracking scheme for PV systems operating under partially shaded conditions," *IEEE Trans. Ind. Electron.*, vol. 55, no. 4, pp. 1689–1698,. 2008.

[6] F. Spertino, A. Ciocia, F. Corona, P. Di Leo and F. Papandrea, "An experimental procedure to check the performance degradation on-site in grid-connected photovoltaic systems," 2014 IEEE 40th Photovoltaic Specialist Conference (PVSC), Denver, CO, 2014, pp. 2600–2604.

[7] J. Feng, H. Wang, J. Xu, M. Su, W. Gui and X. Li, "A Three-Phase Grid-Connected Micro-Inverter for AC PV Module Applications," *IEEE Trans. on Power Electronics*, in press.

[8] Photovoltaics in buildings: a design handbook for architects and engineers. F. Sick, T. Erge, International Energy Agency. Solar Heating and Cooling Programme, Task 16, James & James (Science Publishers) Ltd., 1996.

[9] K. Elkamouny, B. Lakssir, M. Hamedoun, A. Benyoussef and H. Mahmoudi, "Simulation, design and test of a single phase micro inverter for PV application," 2016 International Renewable and Sustainable Energy Conference (IRSEC), Marrakech, 2016, pp. 843–850.

[10] T. Zheng, E.B. Makram and A.A. Girgis, "Evaluating power system unbalance in the presence of harmonic distortion," *IEEE Trans. on Power Delivery*, Vol. 18 (2), pp. 393–397, 2003

[11] R. Langella, A. Testa and A.E. Emanuel, "Unbalance definition for electrical power systems in the presence of harmonics and interharmonics," *IEEE Trans. on Instrum. Meas*., Vol. 61 (10), pp. 2622–2631, 2012.

[12] IEC, 2010. Electromagnetic compatibility (EMC) – Part 4-7: Testing and measurement techniques – General guide on harmonics and interharmonics measurements and instrumentation, for power supply systems and equipment connected thereto, IEC Standard 61000-4-7.

[13] G. Chicco, A. Russo, E. Pons, F. Spertino, R. Porumb, P. Postolache and C. Toader, "Assessment of distortion and unbalance components in three-phase systems with harmonics and interharmonics," *Electric Power Systems Research*, Vol. 147, pp. 201–212, 2017.

[14] A. Ciocia, A. Mazza, A. Russo, F. Spertino and D. Enescu, "Experimental Investigations to Characterize Power Quality of AC Supplied Thermoelectric Refrigerators," 52th International Universities Power Engineering Conference (UPEC), Heraklion, 2017.

[15] IEEE, 2014. IEEE Recommended Practice and Requirements for Harmonic Control in Electric Power Systems, IEEE Standard 519-2014.

[16] G. Chicco, R. Porumb, P. Postolache and C. Toader, "Characterization of unbalanced and distorted distribution systems from experimental data," Melecon 2010 - 2010 15th IEEE Mediterranean Electrotechnical Conference, Valletta, 2010, pp. 154–159.

[17] EN 50160, Voltage characteristics of electricity supplied by public distribution systems, 2011.

[18] G. Chicco, F. Corona, R. Porumb and F. Spertino, "Experimental Indicators of Current Unbalance in Building-Integrated Photovoltaic Systems," *IEEE Journal of Photovoltaics*, vol. 4, pp. 924–934, 2014.

[19] G.Chicco, P.Postolache and C.Toader, "Analysis of three-phase systems with neutral under distorted and unbalanced conditions in the symmetrical component-based framework," *IEEE Trans. on Power Delivery*, vol. 22, No.1, pp. 674–683, 2007.

[20] C.L.Fortescue, “Method of symmetrical coordinates applied to the solution of polyphase networks”, *Trans. AIEE*, pt.II 37, 1027–1140, 1918.

[21] F. Spertino, A. Ciocia, P. Di Leo, R. Tommasini, I. Berardone, M. Corrado, A. Infuso, M. Paggi, “A power and energy procedure in operating photovoltaic systems to quantify the losses according to the causes,” *Solar Energy*, vol. 118, pp. 313-326, 2015.

[22] F. Spertino, G. Graditi, “Power conditioning units in grid-connected photovoltaic systems: A comparison with different technologies and wide range of power ratings, *Solar Energy*, vol. 108, pp. 219-229, 2014.